Supramolecular Chemistry
Publication details, including instructions for authors and subscription information:
http://www.informaworld.com/smpp/title~content=t713649759

Fluoride Ion Receptors: A Comparison of a Polyammonium Monocycle *Versus* its Bicyclic Corollary

Juan A. Aguilar[a]; Thomas Clifford[b]; Andrew Danby[b]; José M. Llinares[b]; Susan Mason[b]; Enrique García-Españ[a]; Kristin Bowman-james[b]
[a] Departamento de of Química Inorgánica, Falcultad de Química, Universidad de Valencia, Burjassot (Valencia), Spain [b] Department of Chemistry, University of Kansas, Lawrence, Kansas

To cite this Article Aguilar, Juan A. , Clifford, Thomas , Danby, Andrew , Llinares, José M. , Mason, Susan , García-Españ, Enrique and Bowman-james, Kristin(2001) 'Fluoride Ion Receptors: A Comparison of a Polyammonium Monocycle *Versus* its Bicyclic Corollary', Supramolecular Chemistry, 13: 3, 405 — 417

To link to this Article: DOI: 10.1080/10610270108029457

URL: http://dx.doi.org/10.1080/10610270108029457

SUPRAMOLECULAR CHEMISTRY, Vol. 13, pp. 405–417
Reprints available directly from the publisher
Photocopying permitted by license only

Fluoride Ion Receptors: A Comparison of a Polyammonium Monocycle *Versus* its Bicyclic Corollary

JUAN A. AGUILAR[a], THOMAS CLIFFORD[b], ANDREW DANBY[b],
JOSÉ M. LLINARES[b], SUSAN MASON[b], ENRIQUE GARCÍA-ESPAÑA[a]
and KRISTIN BOWMAN-JAMES[b,*]

[a]*Departamento de of Química Inorgánica, Falcultad de Química, Universidad de Valencia, C/Dr. Moliner, 50, 46100 Burjassot (Valencia), Spain;*
[b]*Department of Chemistry, University of Kansas, Lawrence, Kansas, 66045*

(Received 13 June 2000)

Two polyammonium macrocyclic receptors, the monocyclic 3,6,9,17,20,23-hexaazatricyclo[23.3.1.1^{11,15}]triaconta-1(29),11,13,15(30),25,27-hexaene (L^1) and its bicyclic analog 1,4,12,15,18,26,31,39-octaazapentacyclo[13.13.13.1^{6,10}.1^{20,24}.1^{33,37}]-tetratetraconta-6,7,9,20(43),21,23,33(42),34,36-nonaene (L^2), have been synthesized as their hexatosylate salts. The propensity for binding fluoride ion was examined using both NMR and potentiometric techniques. The fluoride salts of both receptors have been characterized by X-ray crystallographic methods. For the monocycle, the complex crystallized as the mixed fluoride-bifluoride salt, $[H_6L^1]^{6+} \cdot 4F^- \cdot 2FHF^- \cdot 4H_2O$, and the bicycle crystallized as a complex salt, $[H_6L^2]^{6+} \cdot F^- \cdot 2FHF^- \cdot 1.5SiF_6^{2-} \cdot 7H_2O$.

Keywords: Fluoride; Monocycle; NMR technique; Crystal structure

INTRODUCTION

Anion recognition and binding is an exciting and growing field in receptor chemistry [1–12]. Considerable interest in the area has evolved from analytical, biological, and environmental issues, where anions of all shapes and sizes play major roles. The simplest of anions, and to date the most extensively investigated, are the spherical halides. In fact, halide inclusion complexes of bicyclic katapinands (from the Greek: *καταπιϖω*, swallow-up) reported in 1968 [13] are considered by many to be the first examples of "supramolecular" complexes of anions. These complexes were not structurally characterized until 1975, at which time the crystal structure of the chloride complex of the katapinand with three nine-carbon bridges was published [14].

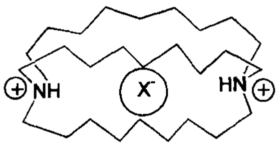

katapinand

---

*Corresponding author. e-mail: kbowman-james@ukans.edu

Of the halides, fluoride, being the smallest, has unique properties compared to its congeners, which are primarily a result of the relative small size and high electronegativity of the fluoride ion. It is also an ion of significant environmental importance, as in the controversial fluoridation of water to prevent tooth decay [15, 16]. While low concentrations of fluoride in water may be beneficial in the latter regard, prolonged high concentrations can produce a mottling of teeth known as dental fluorosis. Excess fluoride in groundwater is often due to contamination by industrial plants that are involved in processing resources with high fluoride content [17]. Hence, more in-depth studies of the binding of fluoride to selective receptor species can potentially lead to applications in wastewater management. A number of receptors for fluoride have been reported [18–29], including both monocycles and bicycles. Monocyclic receptors include tetraamines [18], sapphyrins [19–22], fluorinated crown ethers [23], and calixarenes [24], as well as an interesting tin analog of the katapinands [25], while polyazacryptands are of particular relevance to our studies [26–29].

Our recent interests have focused on the design of agents capable of selective recognition of substrates of environmental significance [29–35]. In doing so we hope to develop new and more efficient analytical techniques for the determination and separation of anions in aqueous environments. In this regard, we have examined the potential of a polyammonium macrocycle and its corollary bicycle [29] as receptors for fluoride. Herein are reported the crystal structures of the fluoride salts of the simple monocycle,3,6,9,17,20,23-hexaazatricyclo [23.3.1.1^{11,15}]-triaconta-1(29),11,13,15(30),-25,27-hexaene (L^1), and its bicyclic counterpart 1,4,12, 15,18,26,31,39-octa-azapentacyclo-[13.13.13.1^{6,10} .1^{20,24} .1^{33,37}]-tetratetraconta-6,7,9, 20(43),21,23, 33(42),-34,36-nonaene (L^2) and the results of the binding studies with fluoride in aqueous solution. Examining the binding modes in the relatively open macromonocyclic structure and the more enclosed bicyclic cryptand has enabled us to compare the properties between "pseudo two-dimensional" and "pseudo three-dimensional" receptors.

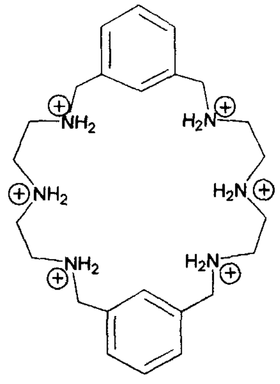

$[H_6L^1]^{6+}$

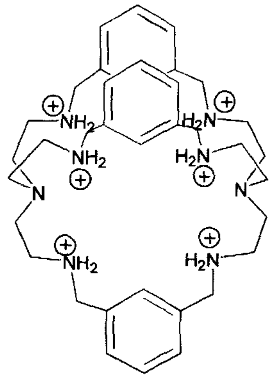

$[H_6L^2]^{6+}$

RESULTS AND DISCUSSION

Crystal Structures

Structure of the Fluoride Complex with L^1 (1)

Crystallographic data for the monocycle and bicycle are provided in Table I. The structure shows two distinct centrosymmetric conformations of the macrocycle (L^{1a} and L^{1b} shown in Fig. 1) arranged in alternating stacks through the lattice. The difference between the two conformations arises from differences in the torsion angles around the C(7)-N(8) bond in L^{1b} and C(22)-N(23) in L^{1a} (Tab. II). The torsion angle for C(6)-C(7)-N(8)-C(9) is −179.7(5)°, *trans*, and for C(21)-C(22)-N(23)-C(24) is 68.2(5)°, *gauche*, for L^{1b} and L^{1a}, respectively. Also a small difference in the C(7)-N(8)-C(9)-C(10) torsion angle for L^{1b} compared to that of C(22)-N(23)-C(24)-C(25) for L^{1a} can be noted. While both are *gauche*, the L^{1b} torsion angle is more acute by approximately 7°, resulting in quite an observable difference in the tilt of the benzene rings between L^{1a} and L^{1b}.

TABLE I Crystallographic data for $H_6L^1 \cdot 4F^- \cdot 2FHF^- \cdot 4H_2O$ (1) and $H_6L^2 \cdot 1.5\ SiF_6^{2-}F^- \cdot 2FHF^- \cdot 7H_2O$(2)

	1	2
Empirical formula	$C_{24}H_{54}N_6O_4F_8$	$N_8C_{36}F_{14}H_{76}O_7Si_{1.5}$
Formula weight	642.72	1041.15
Crystal color, habit	Clear, Prism	Clear, Prism
Crystal dimensions (mm)	0.10 X 0.10 X 0.70	0.20 x 0.30 x 0.50
Crystal system	Triclinic	Triclinic
Space group	$P\bar{1}$(#2)	$P\bar{1}$(#2)
a (Å)	11.268(1)	14.243(2)
b (Å)	15.576(4)	17.128(2)
c (Å)	9.972(2)	11.384(1)
α, deg	105.78(2)	98.68(2)
β, deg	94.44(1)	107.74(2)
γ, deg	71.60(1)	106.73(2)
V (Å^3)	1598.1(6)	2445(1)
Z	2	2
d_{calc} (g/cm^3)	1.336	1.414
γ(Å)	1.5412	1.5412
T(°C)	−100.0	23.0
Reflections collected	3855	7623
Independent reflections	3620	7274
Goodness of fit on F^2	2.24	2.24
$^a R$; $^b R_W$	0.062; 0.059	0.063; 0.061

^{a} $R = \Sigma||F_o| - |F_c||/\Sigma|F_o|$.
^{b} $R_w = [\Sigma w(|F_o| - |F_c|)^2/\Sigma w F_o^2]^{1/2}$.

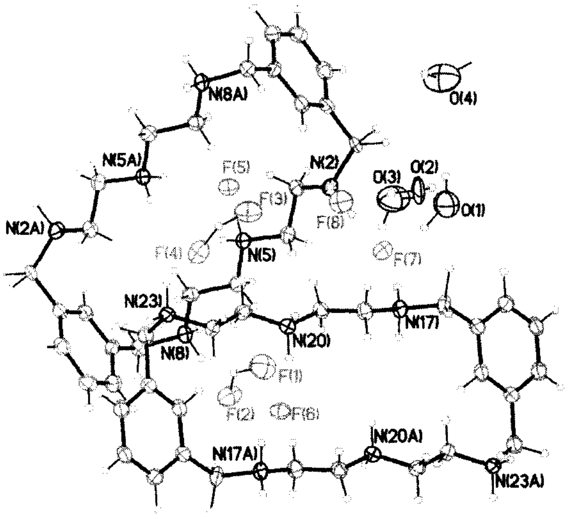

FIGURE 1 ORTEP diagram of **1** showing both L^{1a} and L^{1b} with the numbering scheme and associated anions and water molecules. (See Color Plate I).

Figure 2 shows the intricate packing arrangement in **1** as viewed along the *a* axis. Fluorides occupy the space between macrocycles stacked along the *a* axis and fluorides of adjoining stacks are linked by hydrogen bonded water networks. Careful inspection of connectivities revealed two bifluoride (F-H-F$^-$) anions (F(1)···F(2) = 2.298(5) Å and F(3)···F(4) = 2.268(5) Å) (Tab. III). These distances agree well with those found in other bifluoride structures [36–42]. Bifluorides are situated between the macrocylic layers and are hydrogen bonded to L^{1b} *via* F(2)···N(8) and F(4)···N(5) interactions. The remaining fluorides exhibit extensive hydrogen bonding (Tab. III). F(5) is hydrogen bonded to N(5) of an L^{1b} macrocycle and also to two separate L^{1a} macrocycle nitrogens (N(23) and N(20*)). F(6) is closely associated with two different L^{1a} macrocycles through hydrogen bonds to N(20) and N(17)*, with a third hydrogen bond to N(8) on L^{1b}. The final two fluorides, F(7) and F(8), bridge L^{1a} and L^{1b} through hydrogen bonds: to N(17) (L^{1a}) and N(2) (L^{1b}) for F(7); and N(23) (L^{1a}) and N(2)* (L^{1b}) for F(8). These two fluorides are also linked

TABLE II Selected torsion angles (deg) for L^1

L^{1b}					L^{1a}				
Atom	Atom	Atom	Atom	Angle	Atom	Atom	Atom	Atom	Angle
C(1)	N(2)	C(3)	C(4)	154.4(4)	C(16)	N(17)	C(18)	C(19)	172.9(4)
N(2)	C(3)	C(4)	N(5)	152.9(4)	N(17)	C(18)	C(19)	N(20)	162.6(4)
N(2)	C(1)	C(12A)	C(11A)	58.3(7)	N(17)	C(16)	C(29)	C(28)	102.6(6)
N(2)	C(1)	C(12)	C(13)	−122.8(5)	N(17)	C(16)	C(29)	C(30)	−77.9(6)
C(3)	C(4)	N(5)	C(6)	166.4(4)	C(18)	C(19)	N(20)	C(21)	158.9(4)
C(4)	N(5)	C(6)	C(7)	163.2(4)	C(19)	N(20)	C(21)	C(22)	−176.8(4)
N(5)	C(6)	C(7)	N(8)	173.0(4)	N(20)	C(21)	C(22)	N(23)	178.7(4)
C(6)	C(7)	N(8)	C(9)	−179.7(4)	C(21)	C(22)	N(23)	C(24)	68.2(5)
C(7)	N(8)	C(9)	C(10)	−46.2(6)	C(22)	N(23)	C(24)	C(25)	53.1(6)
N(8)	C(9)	C(10)	C(11)	99.6(6)	N(23)	C(24)	C(25)	C(26)	78.5(6)
N(8)	C(9)	C(10)	C(15)	−82.6(6)	N(23)	C(24)	C(25)	C(30)	−101.7(6)

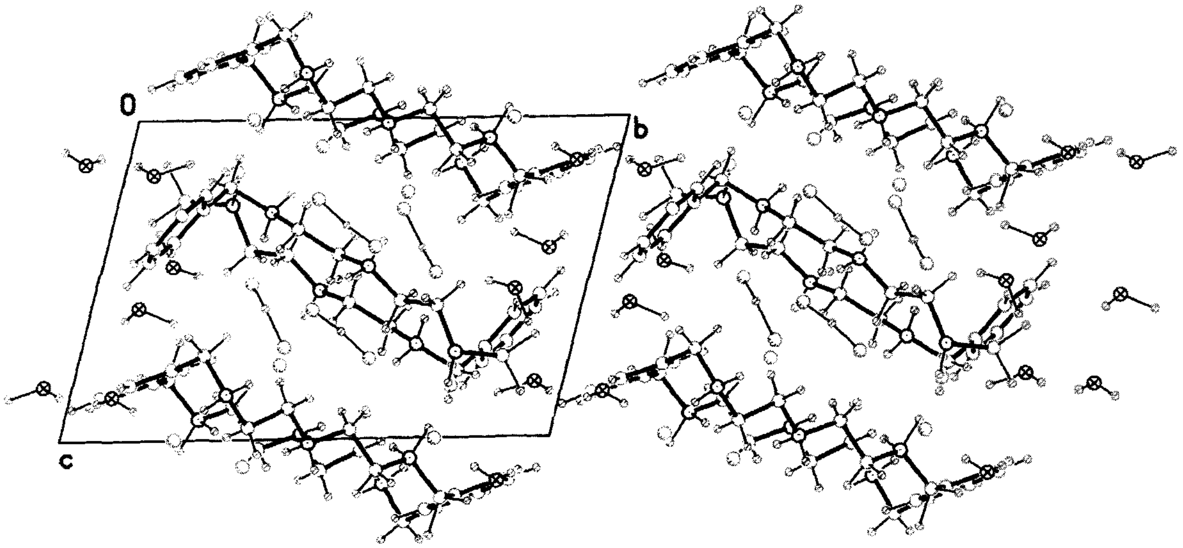

FIGURE 2 Packing diagram of **1** as viewed down the *a* axis. (See Color Plate II).

TABLE III Selected interatomic hydrogen bonding distances (Å) for **1**

FH···F$^-$		F$^-$			
Atoms	Distance	Atoms	Distance	Atoms	Distance
F(1)···F(2)	2.298(5)	F(5)···N(5)	2.600(5)	F(7)···O(1)	2.574(6)
F(3)···F(4)	2.268(5)	F(5)···N(20)*	2.598(5)	F(7)···N(2)	2.591(5)
		F(5)···N(23)*	2.609(5)	F(7)···N(17)	2.588(5)
F(2)···O(3*)	2.720(6)	F(6)···N(8)*	2.620(5)	F(8)···O(2)	2.438(5)
F(2)···N(8)	2.654(6)	F(6)···N(17)*	2.654(5)	F(8)···N(2)	2.780(5)
F(4)···N(5)	2.660(5)	F(6)···N(20)	2.600(5)	F(8)···N(23)*	2.607(5)

* Denotes atom in a unit related by a symmetry operation.

into the hydrogen bonded water array *via* O(1) and O(2) for F(7) and F(8), respectively.

Structure of the Fluoride Complex with L^2 (2)

The electron density maps indicated that two species were in the cavity, but that only one was a fluoride ion, with the other being identified as a molecule of water. The structure of the entire assembly was found to be more complex than anticipated and includes the macrocycle with its inhabitants (the fluoride and water), 1.5 SiF_6^{2-} ions (one dianion sits on the crystallographically imposed inversion center), two bifluoride ions ($F\text{-}H\cdots F^-$), and six external water molecules (Fig. 3). The presence of the SiF_6^{2-} was not anticipated, considering that the reaction was carefully carried out in the absence of glass vessels. However, it may be the result of some contamination of SiF_6^{2-} in the HF. (In previous attempts to isolate a BF_4^- salt of the pyridine analog of **2**, McKee and Nelson found SiF_6^{2-} enclosed within the bicycle) [43].

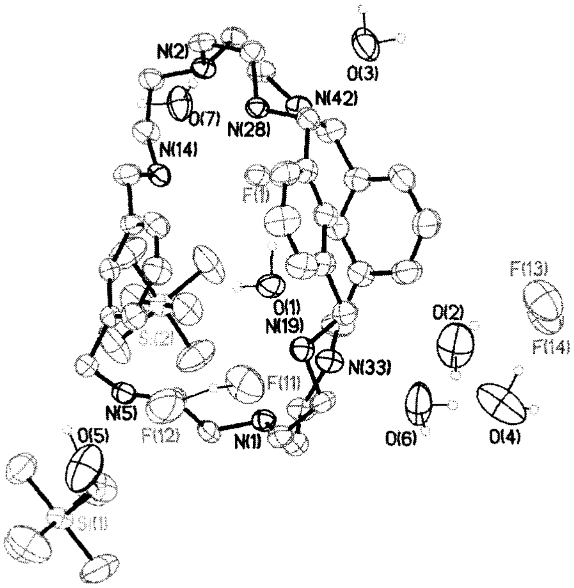

FIGURE 3 ORTEP diagram of **2** showing the numbering scheme and the other associated anions and water molecules. (See Color Plate III).

A perusal of the torsion angles for the bicycle tends to explain the break in symmetry for one of the arms as viewed down the pseudo three-fold axis (Tab. IV). The torsion angles of the chain N(1) through N(5), N(14) to N(2) differ from those of the other two chains. This is evident in the N(1)-C(3)-C(4)-N(5) torsion angle which is closer to a *trans* orientation compared to the *gauche* angles shown for the other two analogous chains, as well as the C(4)-N(5)-C(6)-C(7) and C(13)-N(14)-C(15)-C(16) torsion angles, both of which are *gauche* as opposed to their *trans* counterparts in the other two chains. The *gauche-trans-trans* orientations lead to a very symmetrical pinwheel-like structure if carried out through all three chains, as observed in the nitrate structure of this particular ligand [30].

Figure 4 shows the end-on view of the macrocycle. The encapsulated fluoride and water molecule are shifted from the "central axis" between the two apical nitrogens of the macrocycle toward the "symmetrical" arms as can be seen in the view down the resulting skewed three-fold axis. The internal fluoride, F(1), is tightly held with a short F(1)···N(14) distance of 2.636(5) Å, and sits 2.714(5) Å from N(28) and 2.700(5) Å from N(42) (Tab. V). It could be that the distortion in the N(1)–N(5)–N(14)–N(2) chain is the result of the "misfit" of the very small fluoride in the cavity, such that the chain distorts in order to gain stability *via* a third hydrogen bond with the fluoride. On the other hand, the water molecule shows hydrogen bond contacts both with the internal fluoride (2.842(5) Å) as well as a strong contact with one of the external SiF_6^{2-} counterion fluorides (O(1)···F(9) = 2.693(5) Å). The macrocyclic distortion could, on the other hand, be a result of the "pull" exerted on the water by the external anion, giving a "snapshot" of the mechanism of internal *versus* external water exchange. The consequence is that the part of the macrocyclic cavity containing the water molecule tends to be more open than the other half (Fig. 3).

TABLE IV Selected torsion angles (deg) for L^2

Atom	Atom	Atom	Atom	Angle	Atom	Atom	Atom	Atom	Angle
N(1)	C(3)	C(4)	N(5)	155.3(4)	N(2)	C(16)	C(15)	N(14)	58.7(6)
N(1)	C(17)	C(18)	N(19)	72.2(6)	N(2)	C(30)	C(29)	N(28)	67.5(6)
N(1)	C(31)	C(32)	N(33)	64.4(6)	N(2)	C(44)	C(43)	N(42)	63.3(6)
C(3)	C(4)	N(5)	C(6)	174.2(4)	C(13)	N(14)	C(15)	C(16)	56.4(6)
C(17)	C(18)	N(19)	C(20)	−175.6(4)	C(27)	N(28)	C(29)	C(30)	173.9(5)
C(31)	C(32)	N(33)	C(34)	177.9(5)	C(41)	N(42)	C(43)	C(44)	−168.4(4)
C(4)	N(5)	C(6)	C(7)	50.5(6)	C(9)	C(13)	N(14)	C(15)	166.3(5)
C(18)	N(19)	C(20)	C(21)	−168.6(5)	C(23)	C(27)	N(28)	C(29)	163.5(9)
C(32)	N(33)	C(34)	C(35)	174.2(5)	C(37)	C(41)	N(42)	C(43)	−161.4(5)
N(5)	C(6)	C(7)	C(8)	83.4(6)	N(14)	C(13)	C(9)	C(8)	−71.3(7)
N(19)	C(20)	C(21)	C(22)	−109.3(6)	N(28)	C(27)	C(23)	C(22)	100.2(6)
N(33)	C(34)	C(35)	C(40)	−125.9(6)	N(42)	C(41)	C(37)	C(36)	100.1(6)

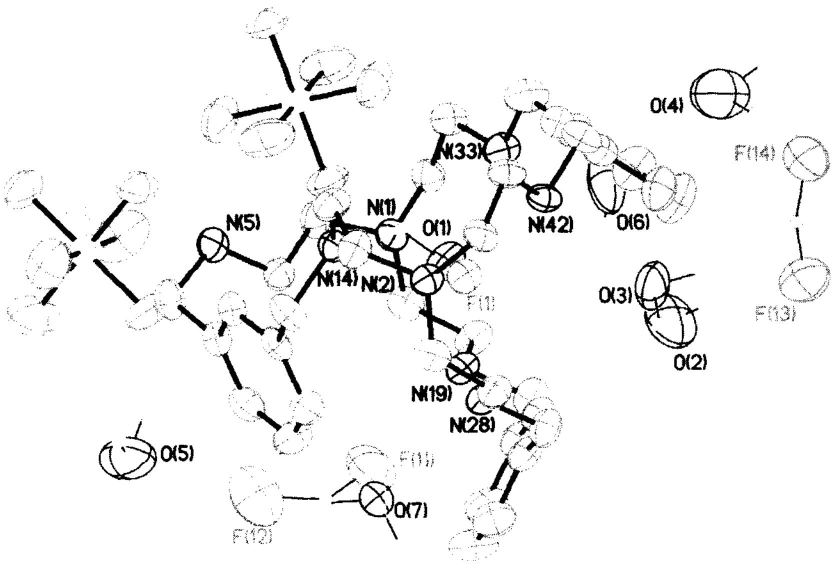

FIGURE 4 ORTEP diagram of **2** as viewed down the "three-fold" axis. (See Color Plate IV).

TABLE V Selected interatomic distances (Å) for **2**

Internal F^-		$FH \cdots F^-$			
Atoms	Distance	Atoms	Distance	Atoms	Distance
F(1)···O(1)	2.814(5)	F(11)···F(12)	2.231(6)	F(11)···O(4)*	2.828(7)
F(1)···N(14)	2.636(5)	F(13)···F(14)	2.277(6)	F(11)···N(19)	2.682(6)
F(1)···N(28)	2.714(5)			F(12)···O(5)	2.828(7)
F(1)···N(42)	2.700(5)			F(13)···O(2)	2.714(7)
				F(13)···O(7)*	2.670(7)
F(1)–N(2)	3.158(5)			F(13)···O(4)	2.725(7)
				F(14)···O(3)*	2.659(6)

* Denotes atom in a unit related by a symmetry operation.

Outside of the macrocycle, the counterions and water molecules are associated with each other *via* hydrogen bonding networks. Identification of the bifluoride anions as distinguished from the water molecules of crystallization was accomplished *via* careful scrutiny of connectivities, which indicated extremely short distances between F(11) and F(12), and F(13) and F(14) (2.231(6) and 2.277(6) Å, respectively). Again, these distances agree well with those found in other bifluoride structures [36–42]. The other peaks found in the electron density maps exhibited longer intramolecular distances (from 2.6–2.8 Å) and were assigned as the oxygen atoms of water molecules. The final assignment of six external water molecules and two bifluoride ions agrees exceptionally well with the microanalysis (*vide infra*). We also observed a similar water hydrogen bond network in the structure of the dinitrate inclusion complex with L^2 and in other structures with these types of receptors [30, 44].

The presence of two species within the macrocycle in L^2 contrasts with the crystal structures of two related macrobicycles, **3** [26] and **4** [27]. The first is known as bis-tren (**3**), and the structure of the fluoride salt shows a single fluoride residing at one end of the cavity with a pseudo-tetrahedral coordination to four protonated nitrogens (including the bridgehead nitrogen), with no other "guests" within the cavity [26]. Interestingly, the authors noted they were hoping for a linear bifluoride ion to reside inside the macrocycle. The fact that the crystal structure of L^2 actually contains bifluorides in the structure, but again not in the cavity, may be an indication that binding of bifluoride inside such a cavity is not favorable.

The other related cryptand (**4**), an octaazacryptand lacking the oxo bridge, is significantly smaller. In this latter case the fluoride is almost the perfect size for the macrocyclic cavity, residing in the center [27, 28]. Of the three cryptand structures, **2**, **3**, and **4**, cryptand **2** exhibits the longest distance between the bridgehead nitrogens, 9.34 Å. That distance is 7.66 and 8.02 Å for the two symmetry unrelated macrocycles in the crystal structure of **3** [26] and 6.65 Å for **4** [27]. However, the distance from the internal fluoride to the nearest nitrogen is 2.636 Å in **2**, which is significantly shorter than the hydrogen bonds in either of the other two bicycles. For bis-tren, **3**, the mean F···N distance is 2.72 Å [26], while in the "ideal" octaazacryptand case **4**, the F···N distances range from 2.76 to 2.88 Å [27].

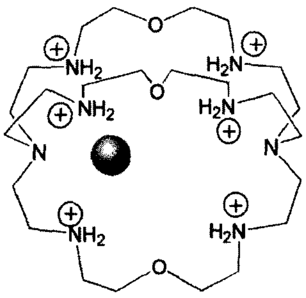

3

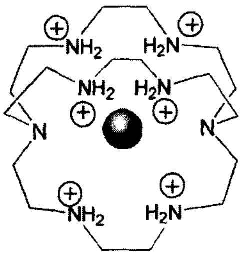

4

Binding Studies

Protonation Constants

The protonation constants of L^1 and L^2 were determined using sodium *p*-toluenesulfonate as supporting electrolyte (Tab. VI). These constants were previously determined by others using other salts and electrolyte conditions [45–48]. Because of our desire to have as little interference as possible from potential complexation with the supporting electrolyte, the *p*-toluenesulfonate salt of the macrocycle and its sodium salt for the electrolyte were used. For L^1, the protonation constants are in relatively good agreement with those determined previously, with the exception that our fifth protonation constant is somewhat higher (4.50) compared with 3.64 [45] and 3.70 [46] observed by the others. However, the general trend of four initial protonation steps, each succeeding step within one pK_a unit of the previous protonation at

TABLE VI Protonation constants and binding constants with fluoride of L^1 and L^2

	log K				
Equilibrium quotient, K	L^1	L^{1a}	L^{1b}	L^2	L^{2c}
Protonation constants					
$[LH]/[L][H]$	9.72(1)[d]	9.49	9.58	9.59(3)	9.92
$[LH_2]/[LH][H]$	8.96(1)	8.73	8.79	9.38(2)	9.26
$[LH_3]/[LH_2][H]$	8.23(1)	8.03	8.08	8.80(2)	8.75
$[LH_4]/[LH_3][H]$	7.51(1)	7.29	7.34	7.48(2)	7.67
$[LH_5]/[LH_4][H]$	4.50(3)	3.64	3.70	6.77(2)	7.16
$[LH_6]/[LH_5][H]$	3.50(2)	3.45	3.37	6.29(2)	6.59
$[LH_6]/[LH_5][H]$				2.85(3)	
Binding constants					
$[LH_2F]/[LH_2][F]$				2.29(5)[e]	
$[LH_3F]/[LH_3][F]$				2.06(7)[e]	
$[LH_4F]/[LH_4][F]$				2.49(7)[e]	
$[LH_5F]/[LH_5][F]$				3.20(3)	
$[LH_6F]/[LH_6][F]$	[~2][f]			3.56(3)	[3.64][f]
$[LH_7F]/[LH_7][F]$				4.29(4)	
$[LH_8F]/[LH_7][HF]$				3.53(8)	

[a] Hydrochloride salt with 0.1 M KNO_3 electrolyte, Ref. [44].
[b] Hydrochloride salt with 0.1 M KNO_3 electrolyte, Ref. [45].
[c] Hydrochloride salt with 0.1 M KNO_3 electrolyte, Ref. [46].
[d] Values in parenthesis are standard deviation in the last significant figure.
[e] The first three observed binding constants are close to the detection limit, and differences are probably not significant.
[f] Brackets denote NMR-determined binding constant.

$pH > 7$, followed by a gap, followed by the last two protonation steps is common for these tren-based systems. This trend is related to the criteria involved in maximum charge separation: after reaching the tetraprotonated state, the addition of protons becomes less favorable, since they must enter within two carbon units of existing positive centers of charge.

For L^2, the protonation constants are also similar to previous determinations [47, 48], but instead of six, we observe a seventh protonation step. Also, protonation constants determined using KNO_3 as supporting electrolyte are undoubtedly affected by the interaction in solution of the polyprotonated bicycle with the nitrate, as also noted by the previous authors. This effect is especially evident for the last four protonation constants. Similar instances of interactions with the electrolyte were also detected by Lehn and coworkers for the azacryptand **3** [27]. They found that when protonation constants for the same macrocycles were calculated in two difference electrolytes, Me_4NCl and the bulky and presumably non-interactive NaTs, a difference of 0.5 pK_a units and more occurred. This difference was observed only for the fifth, sixth, and seventh protonation constants, where the interaction of the multiply positively charged ligand with chloride could be important.

Fluoride Complexation

The complexation constants of fluoride with the two receptors were determined by potentiometric and ^1H NMR techniques and are given in Table VI. Titration of L^1 with fluoride showed only modest changes compared to titrations in the absence of fluoride, indicating only a rather weak binding affinity In fact, the amount of adduct formed for a 1:1 molar ratio is below 5% and occurs over only a small pH range centered at about pH 3. Because the binding is so weak, an approximate binding constant could only be determined using NMR techniques. This weak binding with the large and flexible L^1 is on the same order of magnitude as observed for small aliphatic tetraamines ranging in size from 16-, to 18-, to 20-membered rings ($\log K_s = 1.9$, 2.0 and 2.8, respectively, with KNO_3 as supporting electrolyte) [18]. It is thus evident that fluoride binding in the flexible monocycle is not nearly as ideal as that observed for a more structured macromonocycle, such as is illustrated by the sapphyrin ring. This pentapyrrolic macrocycle maintains a cavity well-suited, size-wise, for incorporation of fluoride and forms a strong complex ($K_s > 10$ [7] in CH_2Cl_2) [21]. An interesting *bis*-calix[4]arene has also been shown to display selective binding for fluoride ion over chloride ($\log K_s = 3.12$ in CD_2Cl_2) [24].

Of specific interest, however, given the higher affinity of the bicycle L^2 toward fluoride is the binding trend associated with fluoride as a function of pH (Tab. VI and Fig. 5). While results indicate some binding for the di-, tri-, and tetra-protonated forms of L^2 at higher pHs, it is clear that significant binding does not occur until the macrocycle is in its penta- and hexa-protonated forms. The maximum value of $\log K_s = 4.29(4)$, observed for the equilibrium $F + H_7L = H_7LF$, occurs at a pH where a significant amount of HF could already exist in solution ($pK_a = 3.15$). This value is comparable to the 4.01 observed by Lehn and co-workers for **3** [26]. The subsequent equilibrium, designated as $HF + H_6L = H_7LF$, with a lower observed constant ($\log K_s = 3.53(8)$) is certainly reflective of HF comprising a major component of the equilibrium mixture. While hydrogen bonding would still be important for HF, the lack of charge on the molecule would diminish the electrostatic contribution and hence weaken the binding. The mitigating effect of fluoride protonation is clearly shown by examining the conditional constants, defined as $K = \Sigma[H_{i+j}LF]/\Sigma[H_iL]\Sigma[H_jF]$. These constants take into

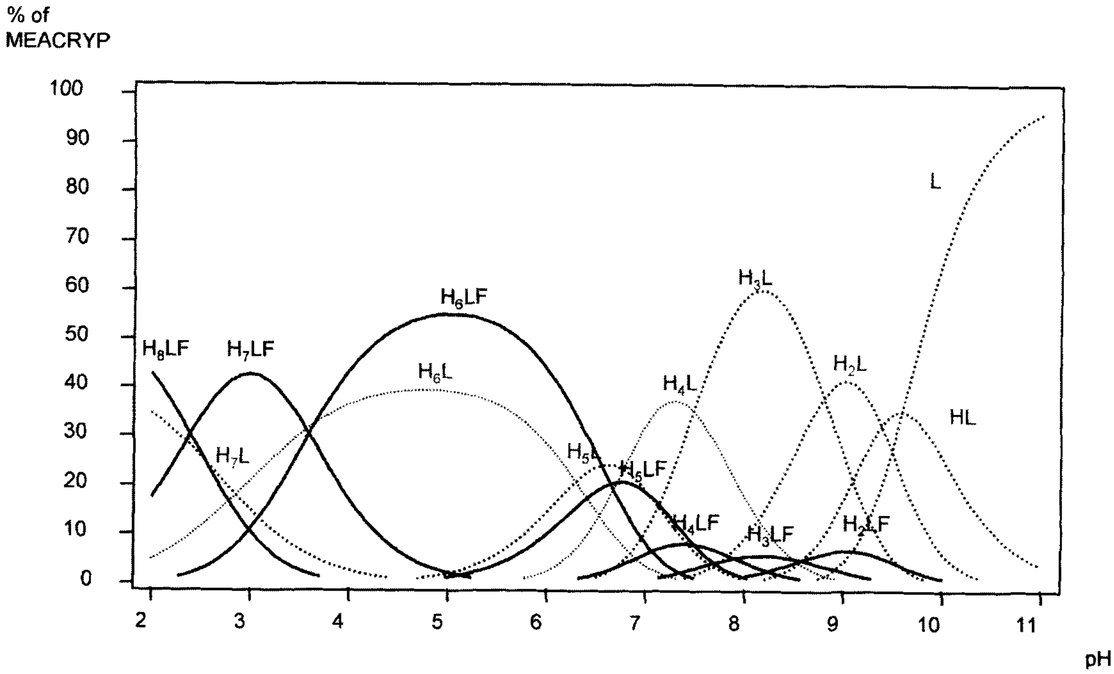

FIGURE 5 Distribution diagram of the tosylate salt of L^2:NaF (1 : 1) in $0.1\,\mathrm{mol\,dm^{-3}}$ of NaTs at 298.1 K.

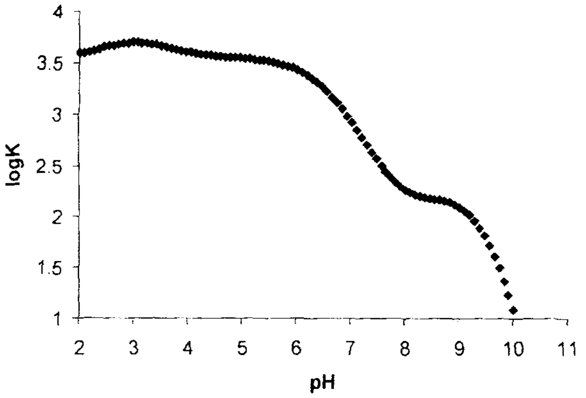

FIGURE 6 Conditional binding constants for a given pH value with $\Sigma[H_iA]$ = total amount of free substrate, $\Sigma[H_jL]$ = total amount of free receptor, and $\Sigma[H_{i+j}AL]$ = total amount of adduct formed, with $K_{eff} = \Sigma[H_{i+j}AL]/\Sigma[H_iA]\Sigma[H_jL]$.

account the presence of both protonation equilibria, that of the macrocycle as well as of fluoride ion, (Fig. 6). The extent of the individual contributions for these equilibria will vary with pH, resulting in conditional constants which never exceed $\log K = 3.6$ Figure 6 also shows clearly the sharp increase of binding commencing at about pH 7.5, with the apparent constant increasing dramatically from about 2.5 to almost 3.5 within one pH unit. This increase could reflect a different mode of binding, namely internal binding of the fluoride. In addition to the crystal structure results, strong, internal binding with L^2 has been further substantiated by ^{19}F NMR techniques, which indicate binding within the cavity for L^2 (signal at −95 ppm) [29] over a significant pH range, including at neutral pHs.

CONCLUSIONS

The crystal structure results for L^1 show an elaborate hydrogen bonding network involving fluorides, bifluorides, water molecules and the protonated macrocycle. The structural results for L^2 represent an unusual finding of two different guests within a single bicyclic host. Binding studies enforce the hypothesis that bicycles are better hosts for anionic substrates compared to more flexible monocyclic analogs. However, while significant binding of fluoride is seen at pHs below 7, we have observed similar affinities of L^2 for other simple anions such as chloride and nitrate [44]. Thus, these receptors may not be optimal for applications such as selective binding. Nonetheless, these studies also clearly point to the utility of these azacryptands as ditopic receptor systems not only for transition metal ions, but also for anions and neutral molecules. Furthermore, the facile synthetic pathway makes these receptors extremely viable candidates for a variety of applications. We are currently investigating the mechanisms of binding, selectivity aspects, and several different applications of these and related macrocycles for anion recognition.

MATERIALS AND METHODS

Materials

NaF (Fisher or Matheson, Coleman, Bell) and HF (Malincrodt) were used without further purification. DMSO-d_6 was obtained from Cambridge Isotope Laboratories, Inc. (Andover, MA). Sodium *p*-toluenesulfonate (NaTs) and *p*-toluenesulfonic acid (TsOH) were purchased from Aldrich and the sodium salt was recrystallized from ethyl ether and dried under vacuum at 50°C [49].

Synthesis

The ligands L^1 and L^2 were prepared by previously reported methods [47,50]. The tosylate salts $L^1 \cdot 6Ts$ [51] and $L^2 \cdot 6Ts$ [52] were prepared by reacting from the corresponding amine in its free base form with *p*-toluenesulfonic acid according to established procedures [26].

$[H_6L^1]^{6+}\cdot 4F^-\cdot 2FHF^-\cdot 4H_2O$ (1)

The hexahydrochloride salt of L^1 (0.9 g, 1.45 mmol) was converted to the free base by ion exchange resin (3×25 column of Dowex 2×B-11) eluting with 50% aqueous ethanol. The solvent was removed at reduced pressure giving the free base as a viscous oil, which was dissolved in a minimum of methanol and transferred to a plastic test tube. Aqueous 48% HF was added until the solution was strongly acidic ($pH < 3$). Most of the solvent was removed at reduced pressure and the hydrogen fluoride salt was precipitated by addition of *iso*-propanol. The filtered solid was recrystallized from hot aqueous ethanol to give colorless plates. Yield 0.447 g, 58%. Anal Calcd for $C_{24}H_{54}N_6O_4F_8$: C, 44.85; H, 8.47; N, 13.08. Found: C, 44.52; H, 8.26; N, 12.96.

$H_6L^2\cdot 1.5SiF_6^{2-}\cdot F^-\cdot 2FHF^-\cdot 7H_2O$ (2)

The hexahydrochloride salt of L^2 (0.2 g, 0.245 mmol) was converted to the free base, and the fluoride complex was prepared in an analogous manner to that of **1**. Yield: 0.116 g, 46%. Anal Calcd for $C_{72}H_{152}N_{16}O_{14}F_{28}Si_3$: C,41.53; H, 7.36; N, 1076. Found C, 41.85; H, 7.47; N, 10.77.

Potentiometric Measurements

Potentiometric titrations were carried out at 298.1 ± 0.1 K in an aqueous solution 0.1 mol dm^{-3} in NaTs. The experimental procedure used has been fully described elsewhere [53]. The acquisition of emf data was performed with the computer program PASAT [54]. The reference electrode was a Ag/AgCl electrode in saturated KCl solution. The glass electrode was calibrated as a hydrogen-ion concentration probe by titration of previously standardized amounts of HCl with CO_2-free NaOH solutions. The equivalence point was determined by Gran's method [55], which gives the standard potential (E°) and the ionic product of water ($pK_w = 13.73(1)$).

The computer program SUPERQUAD [56] was used to calculate the protonation and stability constants. The titration curves for each system consisted of *ca.* 100 experimental points corresponding to at least three measurements. The pH range investigated was 2.5–10.5, and the concentration of the different anions and ligands ranged from 1×10^{-3} to 5×10^{-3} mol dm^{-3}. The protonation constant of fluoride ($\log K_{HF/F\cdot H} = 3.15$) was also redetermined for these measurements.

NMR Experiments

Binding constants using NMR techniques were obtained at 400 MHz on a Bruker AIX400 spectrometer using a presaturation pulse to suppress the water signal. ^1H NMR experiments were run under the same conditions as the potentiometric titrations except that the solutions contained 10% v/v D_2O to ensure a good deuterium lock. The solution pH was maintained at *ca.* 2.5 by small additions of *p*-toluenesulfonic acid or NaOH. Throughout titrations, the pH varied by no more than 0.005 pH units. Changes in the chemical shift ($\Delta\delta$) could be measured for L^1 ($\delta = 3.65$ [m, 16H, $-NCH_2CH_2N-$, $\Delta\delta = 1.03$ Hz], 4.39 [s, 8H, $-NCH_2C_{Ar}$, $\Delta\delta = 1.95$ Hz] and L^2 ($\delta = 2.99$ [t, 12H, $N_{br}(CH_2CH_2N-)_3$, $\Delta\delta = 2.19$ Hz], 3.29 [t, 12H, $N_{br}(CH_2CH_2N-)_3$, $\Delta\delta = 31$ Hz], 4.33 [s, 12Hz, $-NCH_2C_{Ar}$, $\Delta\delta 8.39$]). Twenty points were collected for each titration. The $\Delta\delta$ of the benzyl methylene protons and the fluoride concentration were used in the program EQNMR [57] to compute the formation constants of $[H_6L^1]^{6+}$ and $[H_6L^2]^{6+}$ with fluoride ion.

X-ray Crystal Structure Analysis

X-ray quality crystals of **1** were obtained from a slowly cooled saturated *iso*-propanol solution of the salt. A crystal suitable for X-ray diffraction of **2** was prepared by ether vapor diffusion into a methanolic solution of the fluoride salt.

Crystal data and details of the data collection for **1** and **2** are given in Table I. All measurements were made on a Rigaku AFC5R diffractometer with graphite monochromated Cu-K_α radiation and a rotating anode generator. Reflections were collected to a maximum 2θ value of 104.8° for **1** and 120.1° for **2** by the θ-2θ scan method. The data for which $I > 3.0\sigma(I)$ were corrected for Lorentz and polarization effects, and an empirical absorption correction was made [58] (minimum and maximum transmission coefficients 0.17 and 0.22 for **1** and **2**, respectively). The weak reflections ($I < 2.0\,\sigma(I)$) were rescanned for a maximum of 3 times and the counts were accumulated to ensure good counting statistics. The intensities of three representative reflections were measured every 150 reflections. Over the course of the data collection for **2**, the standards decreased by 4.7%. A linear correction factor was applied to the data for **2**, however, no decay correction was necessary for **1**.

The structures were solved by direct methods and refined by full-matrix least squares techniques on F. Non-hydrogen atoms were refined anisotropically. For **1** hydrogen atoms were generated except for those on the nitrogens, oxygens, fluorides, and phenyl carbons (which were found on the difference maps but not refined). H(32) on O(1) was also generated. For **2** most of the hydrogen atoms on the cryptand, and all of the hydrogens on the waters and bifluorides, were located from difference Fourier maps (minimum and maximum final electron density -0.26 and $0.40\,e^-\,Å^{-3}$ respectively). The weighting scheme was based on counting statistics and included a factor ($p = 0.030$ for **1** and 0.015 for **2**) to downweight the intense reflections. Neutral atom scattering factors were taken from Cromer and Waber [59]. Anomalous dispersion effects were included in F_{calc} [60]. All calculations were performed using the teXan crystallographic software package of Molecular Structure Corporation. Torsion angles and hydrogen bond distances of interest for **1** are given in Tables II and III, respectively, and for **2** in Tables IV and V, respectively.

Acknowledgments

This paper is dedicated on the occasion of his 70th birthday to a revered collaborator, Professor Piero Paoletti, whose many important contributions to the field of macrocyclic chemistry will long be remembered. Support from DOE Grant Number DE-FG07-96ER62307 is gratefully appreciated. The authors acknowledge the support of Dr. Todd Williams of the Mass Spectrometer Laboratory and Dr. David Vander Velde of the NMR Laboratory as well as the X-ray Crystallographic Laboratory at the University of Kansas. Helpful discussions with Dr. Nathaniel W. Alcock are also greatly appreciated.

References

[1] Bianchi, A., Bowman-James, K. and García-España, E., Eds., *Supramolecular Chemistry of Anions*, Wiley-VCH, New York, 1997.

[2] Mertes, M. P. and Mertes, K. B. (1990). *Acc. Chem. Res.*, **23**, 413–418.

[3] Beer, P. D., Wheeler, J. W. and Moore, C. (1992). In: *Supramolecular Chemistry*, Balzani, V. and De Cola, L. (Eds.). Kluwer Academic Publishers, Netherlands, pp. 105–118.

[4] Katz, H. E. (1991). In: *Inclusion Compounds*, Atwood, J. L., Davies, J. E. D. and MacNichol, D. D. (Eds.) Oxford University Press, Oxford, pp. 391–405.

[5] Dietrich, B., Guilhem, J., Lehn, J-M., Pascard, C. and Sonveaux, E. *Helv. Chim. Acta*, **67**, 91–104.

[6] Dietrich, B. (1993). *Pure and Appl. Chem.*, **65**, 1457–1464.

[7] Izatt, R. M., Pawlak, K., Bradshaw, J. S. and Bruening, R. L. (1991). *Chem. Rev.*, **91**, 1721–2085.

[8] Vögtle, F., Sieger, H. and Müller, W. M. (1981). *Top. Curr. Chem.*, **98**, 107–161.

[9] Crompton, T. R., *Determination of Anions*; Springer, New York, 1996.

[10] Kimura, E. (1985). *Top. Curr. Chem.*, **128**, 113–141.

[11] Sessler, J. L., Cyr, M., Furuta, H., Kral, V., Mody, T., Morishma, T., Shionaya, M. and Weghorn, S. (1993). *Pure Appl. Chem.*, **65**, 393–398.

[12] Beer, P. D. and Smith, D. K. (1997). *Prog. Inorg. Chem.*, **46**, 1–96.

[13] Park, C. H. and Simmons, H. E. (1968). *J. Am. Chem. Soc.*, **90**, 2431–2432.

[14] Bell, R. A., Christoph, G. G., Fonczek, F. R. and Marsh, R. E. (1975). *Science*, **190**, 151–152.

[15] Colquhoun, J. (1997). *Perspect. Biol. Med.*, **41**, 29–44.

[16] Diesendorf, M., Colquhoun, J., Spittle, B. J., Everingham, D. N. and Clutterbuck, F. W. (1997). *Austral. N. Z. J. Pub. Health*, **41**, 29–44.

[17] Nomura, J., Imai, H. and Miyake, T., In: *Emerging Technologies in Hazardous Waste Management*, Tedder, D. W. and Pohland, F. G. (Eds.), *ACS Symposium Series 422*, Washington, D.C., 1990.

[18] Suet, E. and Handel, H.(1984). *Tetrahedron Lett.*, **25**, 645–648.

[19] Sessler, J. L., Cyr, M. J., Lynch, V., McGhee, E. and Ibers, J. A. (1990). *J. Am. Chem. Soc.*, **112**, 2810–2813.

[20] Sessler, J. L., Mody, T. D., Ford, D. A. and Lynch, V. (1992). *Angew. Chem., Int. Ed. Engl.*, **31**, 452–455.

[21] Shionoya, M., Furuta, H., Lunch, V., Harriman, A. and Sessler, J. L. (1992). *J. Am. Chem. Soc.*, **114**, 5714–5722.

[22] Sessler, J. L., Cyr, M., Furuta, H., Kral, V., Mody, T., Morishima, T., Shionoya, M. and Weghorn, S. (1993). *Pure and Appl. Chem.*, **65**, 393–398.

[23] Farnham, W. B., Roe, D. C., Dixon, D. A., Calabrese, J. C. and Harlow, R. L. (1990). *J. Am. Chem. Soc.*, **112**, 7707–7718.

[24] Beer, P. D., Gale, P. A. and Hesek, D. (1995). *Tetrahedron Lett.*, **36**, 767–770.

[25] Dietrich, B., Guilhem, J., Lehn, J.-M., Pascard, C. and Sonveaux, E. *Helv. Chim. Acta.*, **67**, 91–104.

[26] Dietrich, B., Lehn, J.-M., Guilhem, J. and Pascard, C. (1989). *Tetrahedron Lett.*, **30**, 4125–4128; Dietrich, B., Dilworth, B., Lehn, J.-M., Souchez, J.-P., Cesario, M., Guilhem, J. and Pascard, C. (1996). *Helv. Chim. Acta*, **79**, 569–587.

[27] Reilly, S. D., Khalsa, R. K., Ford, D. K., Brainard, J. R., Hay, B. P. and Smith, P. H. (1995). *Inorg. Chem.*, **34**, 569–575.

[28] Newcomb, M., Horner, J. H., Blanda, M. T. and Squattrito, P. J. (1989). *J. Am. Chem. Soc.*, **111**, 6294.

[29] Clifford, T., Mason, S., Llinares, J. M. and Bowman-James, K. (2000). *J. Am. Chem. Soc.*, **122**, 1814–1815.

[30] Mason, S., Clifford, T., Seib, L., Kuczera, K. and Bowman-James, K. (1998). *J. Am. Chem. Soc.*, **120**, 8899–8900.

[31] Wiórkiewicz-Kuczera, J., Kuczera, K., Bazzicalupi, C., Bencini, A., Valtancoli, B., Bianchi, A. and Bowman-James, K. (1999). *New J. Chem.*, **23**, 1007–1013.

[32] Gerasimchuk, O. A., Mason, S., Llinares, J. M., Song, M., Alcock, N. W. and Bowman-James, K. (2000). *Inorg. Chem.*, **39**, 1371–1375.

[33] Danby, A., Seib, L., Alcock, N. W. and Bowman-James, K. (2000). *Chem. Commun.*, pp. 973–974.

[34] Kavallieratos, K., Danby, A., Van Berkel, G. J., Kelly, M. A., Sachleben, R. A., Moyer, B. A. and Bowman-James, K. (2000). *Anal. Chem.*, **72**, 5258–5261.

[35] Qian, Q., Wilson, G. S., Bowman-James, K. and Girault, H. H. (2001). *Anal. Chem.*, **73**, 497–503.

[36] McDonald, T. R. R., (1960). *Acta Crystallogr.*, **113**, 113–124.

[37] Frevel, L. K. and Rinn, H. W. (1962). *Acta Crystallogr.*, **15**, 286.

[38] McGaw, B. and Ibers, J. A. (1963). *J. Chem. Phys.*, **39**, 2677–2684.

[39] Ibers, J. A. (1964). *J. Chem. Phys.*, **40**, 402–404.

[40] Williams, J. M. and Schneemeyer, L. F. (1973). *J. Am. Chem. Soc.*, **95**, 5780–5781.

[41] Beno, M. A., Sundell, R. and Williams, J. M. (1984). *Croatica Chem. Acta*, **57**, 695–700.

[42] Farnham, W. B., Dixon, D. A., Middleton, W. J., Calabrese, J. C., Harlow, R. L., Whitney, J. F., Jones, G. A. and Guggenberger, L. J. (1987). *J. Am. Chem. Soc.*, **109**, 476–483.

[43] Morgan, G., McKee, V. and Nelson, J. (1995). *J. Chem. Soc., Chem. Commun.*, pp. 1649–1652.

[44] Aguilar, J. A., Clifford, T., Danby, A., Llinares, J. M., Mason, S., Alcock, N. W., Powell, D., García-España, E. and Bowman-James, K., submitted for publication.

[45] Menif, R., Martell, A. E., Squattrito, P. J. and Clearfield, A. (1990). *Inorg. Chem.*, **29**, 4723–4729.

[46] Basallote, M. G., Durán, J., Fernández-Trujillo, M. J., Máñez, M. A. and Szpoganicz, B. (1999). *J. Chem. Soc., Dalton Trans.*, pp. 1093–1100.

[47] Menif, R., Reibenspies, J. and Martell, A. E. (1991). *Inorg. Chem.*, **30**, 3446–3454.

[48] Arnaud-Neu, F., Fuangswasdi, S., Maubert, B., Nelson, J. and McKee, V. (2000). *Inorg. Chem.*, **39**, 573–579.

[49] *Purification of Laboratory Chemicals.* Perrin, D. D. and Armarego, W. L. F. (Eds.), 3rd edition. Pergamon Press, New York, 1988, p. 352.

[50] Chen, D. and Martell, A. E. (1991). *Tetrahedron*, **47**, 6895–6902.

[51] Anal Calcd **1**·6TsH ($C_{66}H_{86}N_6S_6O_{18}$): C, 54.90; H, 6.00; N, 5.82; S, 13.32. C/N, 9.43; N/H, 0.969. Found C, 53.0; H, 6.02; N, 5.58; S, 12.4. C/N, 9.48; N/H, 0.969.

[52] Anal Calcd **2**·6TsH ($C_{78}H_{102}N_8S_6O_{18}$): C, 57.40; H, 6.29; N, 6.86; S, 11.79. C/N, 8.36; N/H, 1.09. Found C, 56.9; H, 6.23; N, 6.86; S, 11.30. C/N, 8.29; N/H, 1.10.

[53] García-España, E., Ballester, M.-J., Lloret, F., Moratal, J.-M., Faus, J. and Bianchi, A. (1988). *J. Chem. Soc. Daltons Trans.*, pp. 101–104.

[54] Fontanelli, M. and Micheloni, M., *Proceedings of the I Spanish-Italian Congress on Thermodynamics of Metal Complexes*, Diputación de Castellón, Castellon, Spain, 1990.

[55] Gran, G. (1952). *Analyst (London)*, **77**, 881; Rossotti, F. J. C. and Rossotti, H. (1965). *J. Chem. Ed.*, **42**, 375–378.

[56] Gans, P., Sabatini, A. and Vacca, A. (1985). *J. Chem. Soc. Dalton Trans.*, pp. 1195–1200.

[57] Hynes, M. J. (1993). *J. Chem. Soc., Dalton Trans.*, pp. 311–312.

[58] Walker, N. and Stuart, D. (1983). *Acta Crystallogr.*, **A39**, 158–166.

[59] *International Tables for X-ray Crystallography*, Cromer, D. T. and Waber, J. T. (Eds.), The Kynoch Press: Birmingham, England, 1974, Vol. IV, Table 2.2 A.

[60] Ibers, J. A. and Hamilton, W. C. (1964). *Acta Crystallogr.*, **17**, 781.